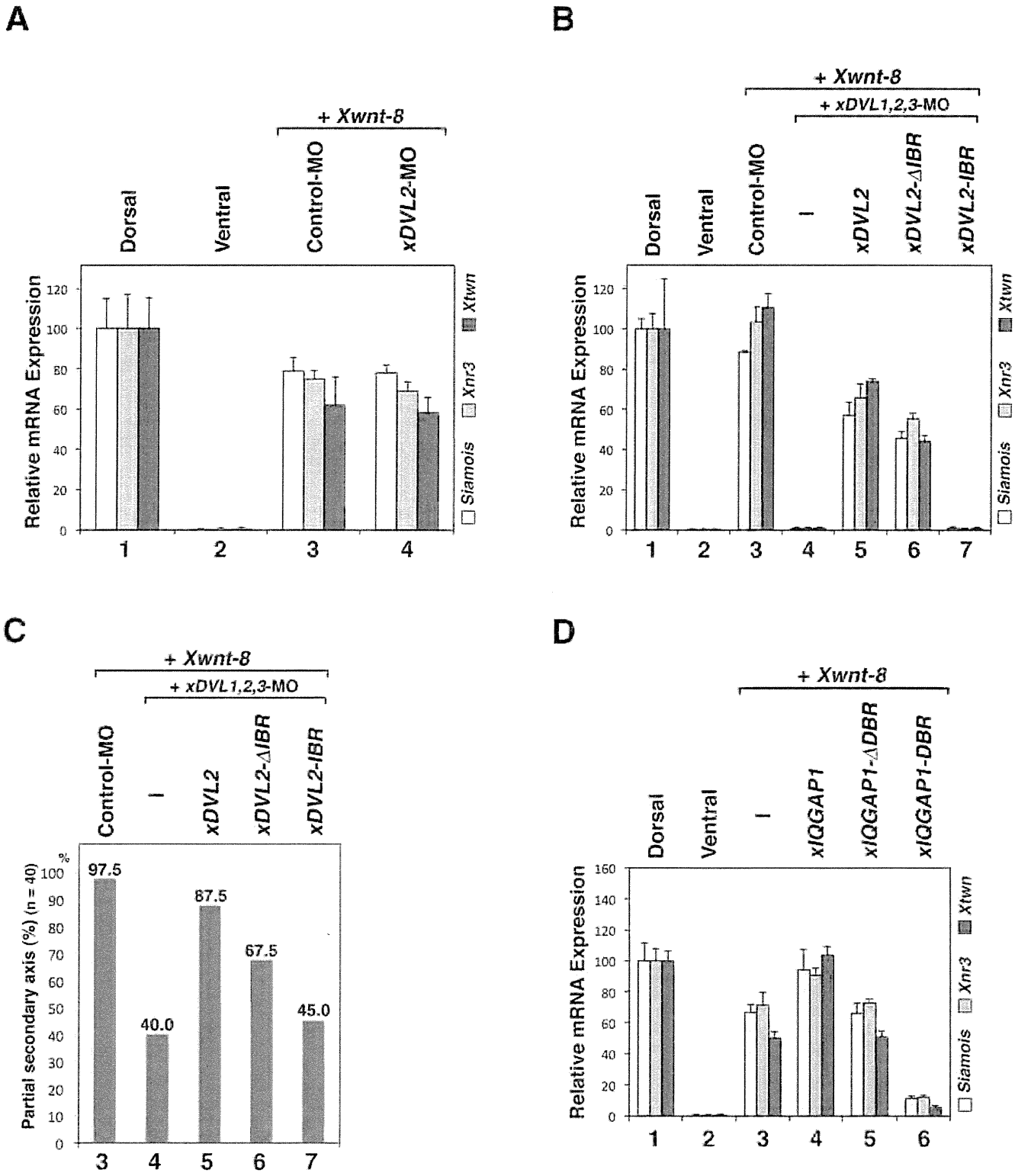

Figure 5. The role of the xIQGAP1-binding region of xDVL2 in canonical Wnt signaling during early embryogenesis. (**A**) Quantitative RT-PCR analysis of early dorsal Wnt target genes (n = 3). Control-MO (15 ng) or *xDVL2*-MO (15 ng) was ventrally co-injected with *Xwnt-8* (0.5 pg) mRNA. RNAs from dissected ventral sectors of injected embryos were extracted at stage 10. The following procedure is indicated in Figure 4A. Error bars represent standard deviation of the mean in three experiments. Statistical significance was determined by Student's *t*-test for each marker gene. The highest P values in three marker genes were chosen as a representative, as follows: $P>0.1$ [between lane 3 and lane 4]. (**B**) Quantitative RT-PCR analysis of early dorsal Wnt target genes (n = 3). *xDVL1*-MO (10 ng), *xDVL2*-MO (10 ng), *xDVL3*-MO (10 ng) and *Xwnt-8* (0.5 pg) mRNA were ventrally co-injected with *xDVL2* constructs: *xDVL2* (25 pg), *xDVL2-ΔIBR* (25 pg), *xDVL2-IBR* (25 pg) mRNA. RNAs from dissected ventral sectors of injected embryos were extracted at stage 10. The following procedure is indicated in Figure 4A. $P<0.05$ [between lane 3 and lane 4], $P<0.05$ [between lane 4 and lane 5], $P<0.1$ [between lane 5 and lane 6], $P<0.05$ [between lane 5 and lane 7]. (**C**) The ratio of injected embryos that exhibited a partial

secondary axis. The numbered lanes indicate the injected mRNAs and MOs consistent with the numbering in Figure B. (**D**) Quantitative RT-PCR analysis of early dorsal Wnt target genes (n = 3). *Xwnt-8* (0.5 pg) mRNA was ventrally co-injected with *xIQGAP1* constructs: *xIQGAP1* (400 pg), *xIQGAP1-ΔDBR* (1 ng), *xIQGAP1-DBR* (1 ng) mRNA. The following procedure is indicated in Figure 4A. P<0.01 [between lane 3 and lane 4], P>0.1 [between lane 3 and lane 5], P<0.05 [between lane 3 and lane 6].
doi:10.1371/journal.pone.0060865.g005

differences among IQGAP isoforms. Further molecular analyses will be needed to clarify the different roles of IQGAP isoforms.

Supporting Information

Figure S1 Expression of *Xenopus* DVL and IQGAP1 isoforms and confirmation of the morpholino specificity. Reverse transcription–polymerase chain reaction analysis was performed using total RNA extracted from *Xenopus* embryos at different stages of development and from different regions. *Ornithine decarboxylase* (*ODC*) was used as an internal control. (**A**) Temporal expression patterns. U, unfertilized eggs. The numbers indicate developmental stages. (**B**) Spatial expression patterns. Embryos were dissected at stage 10, and dissections were performed as shown in the right panel. D, dorsal; Vn, ventral; A, animal; M, marginal; Vg, vegetal; H, head. (**C**) Morpholino (MO) (10 ng) and FLAG-tagged mRNAs (100 pg) were co-injected with *β-globin-FLAG* mRNA (100 pg) as loading control into the animal poles of 4-cell stage embryos, and the injected animal caps were dissected at stage 10. Lysates from the animal caps were subjected to Western blotting with anti-FLAG antibody (M2, Sigma).
(TIF)

Figure S2 Localization of xDVL2 and xIQGAP1 GFP constructs in *Xenopus* animal cap cells at stage 10. (**A**) GFP signals (left panels). DAPI staining (center panels). Merge (right panels). xDVL2-ΔIBR-GFP (upper panels). xDVL2-IBR-GFP (second panels). xIQGAP1-ΔDBR-GFP (third panels). xIQGAP1-DBR-GFP (bottom panels). (**B-E**) The ratio of cells that had nuclear fluorescence signals. The average of ratio was taken with six explants in 3 independent experiments (See Materials and Methods). Error bars represent standard deviation of the mean with six explants. Statistical significance was determined by Student's *t*-test. (**B**) The ratio of nuclear-localized xDVL2-ΔIBR-GFP. Lane 1: n = 499, 22.4%, lane 2: n = 349, 23.8%. P>0.1 [between lane 1 and lane 2]. (**C**) The ratio of nuclear-localized xDVL2-IBR-GFP. Lane 1: n = 740, 78.9%, lane 2: n = 420, 87.6%. P>0.1 [between lane 1 and lane 2]. (**D**) The ratio of nuclear localized xIQGAP1-ΔDBR-GFP. Lane 1: n = 1205, 13.0%, lane 2: n = 410, 14.6%. P>0.1 [between lane 1 and lane 2]. (**e**) The ratio of nuclear localized xIQGAP1-DBR-GFP. Lane 1: n = 1598, 80.6%, lane 2: n = 408, 92.7%. P<0.01 [between lane 1 and lane 2].
(TIF)

Figure S3 Effects of over-expression of *xIQGAP1* and *xDVL2* constructs on the nuclear localization of xDVL2-GFP and xIQGAP1-GFP. The ratio of cells that had nuclear fluorescence signals. The average of ratio was taken with six explants in 3 independent experiments (See Materials and Methods). Error bars represent standard deviation of the mean with six explants. Statistical significance was determined by Student's *t*-test. (**A**) The ratio of nuclear-localized xDVL2-GFP in cells expressing various *xIQGAP1* constructs: *xIQGAP1*, *xIQGAP1-ΔDBR* or *xIQGAP1-DBR* mRNA. Lane 1: n = 1038, 22.1%, lane 2: n = 495, 31.1%, lane 3: n = 698, 26.5%, lane 4: n = 262, 55.7%, lane 5: n = 1171, 41.8%, lane 6: n = 655, 52.7%, lane 7: n = 611, 27.7%, lane 8: n = 520, 61.0%. P<0.1 [between lane 1 and lane 2], P>0.1 [between lane 1 and lane 3], P<0.01 [between lane 1 and lane 4], P<0.01 [between lane 5 and lane 6], P<0.01 [between lane 5 and lane 7], P<0.01 [between lane 5 and lane 8]. (**B**) The ratio of nuclear localized xIQGAP1-GFP in cells expressing various *xDVL2* constructs: *xDVL21*, *xDVL21-ΔIBR* or *xDVL2-IBR* mRNA. Lane 1: n = 801, 22.0%, lane 2: n = 726, 23.3%, lane 3: n = 765, 21.4%, lane 4: n = 1223, 22.2%, lane 5: n = 1171, 36.5%, lane 6: n = 362, 37.6%, lane 7: n = 641, 22.3%, lane 8: n = 549, 33.2%. P>0.1 [between lane 1 and lane 2], P>0.1 [between lane 1 and lane 3], P>0.1 [between lane 1 and lane 4], P>0.1 [between lane 5 and lane 6], P<0.01 [between lane 5 and lane 7], P>0.1 [between lane 5 and lane 8].
(TIF)

Figure S4 The effects of xIQGAP isoforms and xIQGAP1 mutated constructs. (**A, C**) Quantitative RT-PCR analysis of early dorsal Wnt target genes (n = 3). *xIQGAP1*-MO (15 ng) and *xDVL2* (50 pg) or *β-catenin* (20 pg) mRNA were ventrally co-injected with *xIQGAP1* constructs: *xIQGAP1* (400 pg), *xIQGAP1-ΔDBD* (400 pg), *xIQGAP1-DBD* (400 pg) mRNA. RNAs from dissected ventral sectors of injected embryos were extracted at stage 10. RNAs from dissected dorsal and ventral sectors of uninjected embryos were used as controls. The value obtained for each gene was normalized to the level of ODC (ornithine decarboxylase). The value of dorsal sectors was set to 100 and other values were computed. Error bars represent standard deviation of the mean in three experiments. Statistical significance was determined by Student's *t*-test for each marker gene. The highest P values in three marker genes were chosen as a representative. (**A**) P<0.05 [between lane 3 and lane 4], P<0.05 [between lane 4 and lane 5], P<0.05 [between lane 5 and lane 6], P<0.05 [between lane 5 and lane 7]. (**C**) P<0.05 [between lane 3 and lane 4], P<0.05 [between lane 4 and lane 5], P<0.05 [between lane 5 and lane 6], P<0.05 [between lane 5 and lane 7]. (**B, D**) The ratio of injected embryos exhibiting a partial secondary axis. The numbered lanes indicate the injected mRNAs and MOs consistent with the numbering in Figure **A** and **C**, respectively.
(TIF)

Figure S5 The effects of *IQGAP1* on the Wnt target genes in cultured cells. RT-PCR analysis of Wnt target genes in NIH3T3 cells. The transfected cultured cells were stimulated with the Wnt-3A conditioned medium from L-Wnt-3A cells for 24 hours. The condition medium from L cells was used for unstimulated control. GAPDH was used for normalization of cDNA samples. (**A**) siRNAs were transfected. (**B**) xIQGAP1 or xIQGAP1-DBD was transfected.
(TIF)

Figure S6 The effects of xDVL2 and xIQGAP1 mutated constructs. (**A, B**) Quantitative RT-PCR analysis of early dorsal Wnt target genes (n = 3). *xDVL2* (50 pg) or *β-catenin* (20 pg) mRNA were ventrally co-injected with *xIQGAP1* constructs: *xIQGAP1* (400 pg), *xIQGAP1-ΔDBD* (1 ng), *xIQGAP1-DBD* (1 ng) mRNA. The following procedure is indicated in Figure S4A. (**A**) P<0.1 [between lane 3 and lane 4], P<0.05 [between lane 3 and lane 5], P<0.05 [between lane 3 and lane 6]. (**B**) P<0.05 [between lane 3 and lane 4], P>0.1 [between lane 3 and lane 5], P<0.05 [between lane 3 and lane 6].
(TIF)

Acknowledgments

We thank M. Lamphier for critical reading of the manuscript.

Author Contributions

Conceived and designed the experiments: HS . Performed the experiments: TG AS MS SA KS. Analyzed the data: TG AS MS SA KS. Contributed reagents/materials/analysis tools: SI TN. Wrote the paper: HS TG.

References

1. Logan CY, Nusse R (2004) The Wnt signaling pathway in development and disease. Annu Rev Cell Dev Biol 20: 781–810.
2. Clevers H (2006) Wnt/beta-catenin signaling in development and disease. Cell 127: 469–480.
3. Peifer M, Polakis P (2000) Wnt signaling in oncogenesis and embryogenesis–a look outside the nucleus. Science 287: 1606–1609.
4. Wodarz A, Nusse R (1998) Mechanisms of Wnt signaling in development. Annu Rev Cell Dev Biol 14: 59–88.
5. Bienz M, Clevers H (2000) Linking colorectal cancer to Wnt signaling. Cell 103: 311–320.
6. Gumbiner BM (1997) Carcinogenesis: a balance between beta-catenin and APC. Curr Biol 7: R443–R446.
7. Miller JR, Moon RT (1997) Analysis of the signaling activities of localization mutants of beta-catenin during axis specification in *Xenopus*. J Cell Biol 139: 229–243.
8. Sokol S, Christian JL, Moon RT, Melton DA (1991) Injected Wnt RNA induces a complete body axis in *Xenopus* embryos. Cell 67: 741–752.
9. Funayama N, Fagotto F, McCrea P, Gumbiner BM (1995) Embryonic axis induction by the armadillo repeat domain of beta-catenin: evidence for intracellular signaling. J Cell Biol 128: 959–968.
10. Fagotto F, Funayama N, Gluck U, Gumbiner BM (1996) Binding to cadherins antagonizes the signaling activity of beta-catenin during axis formation in *Xenopus*. J Cell Biol 132: 1105–1114.
11. Sokol SY (1996) Analysis of Dishevelled signalling pathways during *Xenopus* development. Curr Biol 6: 1456–1467.
12. Carnac G, Kodjabachian L, Gurdon JB, Lemaire P (1996) The homeobox gene Siamois is a target of the Wnt dorsalisation pathway and triggers organiser activity in the absence of mesoderm. Development 122: 3055–3065.
13. Glinka A, Delius H, Blumenstock C, Niehrs C (1996) Combinatorial signalling by Xwnt-11 and Xnr3 in the organizer epithelium. Mech Dev 60: 221–231.
14. Laurent MN, Blitz IL, Hashimoto C, Rothbächer U, Cho KW (1997) The *Xenopus* homeobox gene twin mediates Wnt induction of goosecoid in establishment of Spemann's organizer. Development 124: 4905–4916.
15. Klingensmith J, Yang Y, Axelrod JD, Beier DR, Perrimon N, et al. (1996) Conservation of dishevelled structure and function between flies and mice: isolation and characterization of Dvl2. Mech Dev 58: 15–26.
16. Pizzuti A, Amati F, Calabrese G, Mari A, Colosimo A, et al. (1996) cDNA characterization and chromosomal mapping of two human homologues of the Drosophila dishevelled polarity gene. Hum Mol Genet 5: 953–358.
17. Lee YN, Gao Y, Wang HY (2008) Differential mediation of the Wnt canonical pathway by mammalian Dishevelleds-1, -2, and -3. Cell Signal 20: 443–452.
18. Capelluto DG, Kutateladze TG, Habas R, Finkielstein CV, He X, et al. (2002) The DIX domain targets dishevelled to actin stress fibres and vesicular membranes. Nature 419: 726–729.
19. Pan WJ, Pang SZ, Huang T, Guo HY, Wu D, et al. (2004) Characterization of function of three domains in dishevelled-1: DEP domain is responsible for membrane translocation of dishevelled-1. Cell Res 14: 324–330.
20. Moriguchi T, Kawachi K, Kamakura S, Masuyama N, Yamanaka H, et al. (1999) Distinct domains of mouse dishevelled are responsible for the c-Jun N-terminal kinase/stress-activated protein kinase activation and the axis formation in vertebrates. J Biol Chem 274: 30957–30962.
21. Rothbächer U, Laurent MN, Deardorff MA, Klein PS, Cho KW, et al. (2000) Dishevelled phosphorylation, subcellular localization and multimerization regulate its role in early embryogenesis. EMBO J 19: 1010–1022.
22. Axelrod JD, Miller JR, Shulman JM, Moon RT, Perrimon N (1998) Differential recruitment of Dishevelled provides signaling specificity in the planar cell polarity and Wingless signaling pathways. Genes Dev 12: 2610–2622.
23. Boutros M, Paricio N, Strutt DI, Mlodzik M (1998) Dishevelled activates JNK and discriminates between JNK pathways in planar polarity and wingless signaling. Cell 94: 109–118.
24. Gan XQ, Wang JY, Xi Y, Wu ZL, Li YP, et al. (2008) Nuclear Dvl, c-Jun, beta-catenin, and TCF form a complex leading to stabilization of beta-catenin-TCF interaction. J Cell Biol 180: 1087–1100.
25. Kuroda S, Fukata M, Kobayashi K, Nakafuku M, Nomura N, et al. (1996) Identification of IQGAP as a putative target for the small GTPases, Cdc42 and Rac1. J Biol Chem 271: 23363–23367.
26. Joyal JL, Annan RS, Ho YD, Huddleston ME, Carr SA, et al. (1997) Calmodulin modulates the interaction between IQGAP1 and Cdc42. Identification of IQGAP1 by nanoelectrospray tandem mass spectrometry. J Biol Chem 272: 15419–15425.
27. Erickson JW, Cerione RA, Hart MJ (1997) Identification of an actin cytoskeletal complex that includes IQGAP and the Cdc42 GTPase. J Biol Chem 272: 24443–24447.
28. Weissbach L, Bernards A, Herion DW (1998) Binding of myosin essential light chain to the cytoskeleton-associated protein IQGAP1. Biochem Biophys Res Commun 251: 269–276.
29. Mateer SC, McDaniel AE, Nicolas V, Habermacher GM, Lin MJ, et al. (2002) The mechanism for regulation of the F-actin binding activity of IQGAP1 by calcium/calmodulin. J Biol Chem 277: 12324–12333.
30. Li Z, Sacks DB (2003) Elucidation of the interaction of calmodulin with the IQ motifs of IQGAP1. J Biol Chem 278: 4347–4352.
31. Roy M, Li Z, Sacks DB (2004) IQGAP1 binds ERK2 and modulates its activity. J Biol Chem 279: 17329–17337.
32. Li Q, Stuenkel EL (2004) Calcium negatively modulates calmodulin interaction with IQGAP1. Biochem Biophys Res Commun 317: 787–795.
33. Kuroda S, Fukata M, Nakagawa M, Fujii K, Nakamura T, et al. (1998) Role of IQGAP1, a target of the small GTPases Cdc42 and Rac1, in regulation of E-cadherin- mediated cell-cell adhesion. Science 281: 832–835.
34. Briggs MW, Li Z, Sacks DB (2002) IQGAP1-mediated stimulation of transcriptional co-activation by beta-catenin is modulated by calmodulin. J Biol Chem 277: 7453–7465.
35. Brown MD, Sacks DB (2006) IQGAP1 in cellular signaling: bridging the GAP. Trends Cell Biol 16: 242–249.
36. White CD, Brown MD, Sacks DB (2009) IQGAPs in cancer: a family of scaffold proteins underlying tumorigenesis. FEBS Lett 583: 1817–1824.
37. Schmidt VA, Chiariello CS, Capilla E, Miller F, Bahou WF (2008) Development of hepatocellular carcinoma in Iqgap2-deficient mice is IQGAP1 dependent. Mol Cell Biol 28: 1489–1502.
38. Yamashiro S, Noguchi T, Mabuchi I (2003) Localization of two IQGAPs in cultured cells and early embryos of *Xenopus laevis*. Cell Motil Cytoskeleton 55: 36–50.
39. Yamashiro S, Abe H, Mabuchi I (2007) IQGAP2 is required for the cadherin-mediated cell-to-cell adhesion in *Xenopus laevis* embryos. Dev Biol 308: 485–493.
40. Itoh K, Brott BK, Bae GU, Ratcliffe MJ, Sokol SY (2005) Nuclear localization is required for Dishevelled function in Wnt/beta-catenin signaling. J Biol 4: 3.
41. Shimizu K, Gurdons JB (1999) A quantitative analysis of signal transduction from activin receptor to nucleus and its relevance to morphogen gradient interpretation. Proc Natl Acad Sci U S A 96: 6791–6796.
42. Ohnishi E, Goto T, Sato A, Kim MS, Iemura S, et al. (2010) Nemo-like kinase, an essential effector of anterior formation, functions downstream of p38 mitogen-activated protein kinase. Mol Cell Biol 30: 675–683.
43. Sato A, Shibuya H (2013) WNK Signaling Is Involved in Neural Development via Lhx8/Awh Expression. PLoS One 8: e55301.
44. Natsume T, Yamauchi Y, Nakayama H, Shinkawa T, Yanagida M, et al. (2002) A direct nanoflow liquid chromatography-tandem mass spectrometry system for interaction proteomics. Anal Chem 74: 4725–4733.
45. Bryja V, Schulte G, Arenas E (2007) Wnt-3a utilizes a novel low dose and rapid pathway that does not require casein kinase 1-mediated phosphorylation of Dvl to activate beta-catenin. Cell Signal 19: 610–616.
46. Song DH, Sussman DJ, Seldin DC (2000) Endogenous protein kinase CK2 participates in Wnt signaling in mammary epithelial cells. J Biol Chem 275: 23790–23797.
47. Bastock R, Strutt H, Strutt D (2003) Strabismus is asymmetrically localised and binds to Prickle and Dishevelled during Drosophila planar polarity patterning. Development 130: 3007–3014.
48. Sun TQ, Lu B, Feng JJ, Reinhard C, Jan YN, et al. (2001) PAR-1 is a Dishevelled-associated kinase and a positive regulator of Wnt signalling. Nat Cell Biol 3: 628–636.
49. Schwarz-Romond T, Metcalfe C, Bienz M (2007) Dynamic recruitment of axin by Dishevelled protein assemblies. J Cell Sci 120: 2402–2412.
50. Strovel ET, Wu D, Sussman DJ (2000) Protein phosphatase 2Calpha dephosphorylates axin and activates LEF-1-dependent transcription. J Biol Chem 275: 2399–2403.
51. Hamblet NS, Lijam N, Ruiz-Lozano P, Wang J, Yang Y, et al. (2002) Dishevelled 2 is essential for cardiac outflow tract development, somite segmentation and neural tube closure. Development 129: 5827–5838.
52. Etheridge SL, Ray S, Li S, Hamblet NS, Lijam N, et al. (2008) Dishevelled 3 Functions in Redundant Pathways with Dishevelled 1 and 2 in Normal Cardiac Outflow Tract, Cochlea, and Neural Tube Development. PLoS Genet 4: e1000259.

JVI
Journals ASM.org

The Host Protease TMPRSS2 Plays a Major Role in *In Vivo* Replication of Emerging H7N9 and Seasonal Influenza Viruses

Kouji Sakai,[a] Yasushi Ami,[b] Maino Tahara,[a] Toru Kubota,[a] Masaki Anraku,[a] Masako Abe,[a] Noriko Nakajima,[c] Tsuyoshi Sekizuka,[d] Kazuya Shirato,[a] Yuriko Suzaki,[b] Akira Ainai,[e] Yuichiro Nakatsu,[a] Kazuhiko Kanou,[f] Kazuya Nakamura,[e] Tadaki Suzuki,[c] Katsuhiro Komase,[a] Eri Nobusawa,[e] Katsumi Maenaka,[g] Makoto Kuroda,[d] Hideki Hasegawa,[c] Yoshihiro Kawaoka,[h,i,j] Masato Tashiro,[e] Makoto Takeda[a]

Department of Virology 3,[a] Division of Experimental Animal Research,[b] and Influenza Virus Research Center,[e] National Institute of Infectious Diseases, Tokyo, Japan; Department of Pathology,[c] Laboratory of Bacterial Genomics, Pathogen Genomics Center,[d] and Infectious Disease Surveillance Center,[f] National Institute of Infectious Diseases, Tokyo, Japan; Laboratory of Biomolecular Science, Faculty of Pharmaceutical Sciences, Hokkaido University, Hokkaido, Japan[g]; Division of Virology, Department of Microbiology and Immunology, and International Research Center for Infectious Diseases, Institute of Medical Science, The University of Tokyo, Tokyo, Japan[h]; ERATO Infection-Induced Host Responses Project, Japan Science and Technology Agency, Saitama, Japan[i]; Influenza Research Institute, University of Wisconsin—Madison, Madison, Wisconsin, USA[j]

ABSTRACT

Proteolytic cleavage of the hemagglutinin (HA) protein is essential for influenza A virus (IAV) to acquire infectivity. This process is mediated by a host cell protease(s) *in vivo*. The type II transmembrane serine protease TMPRSS2 is expressed in the respiratory tract and is capable of activating a variety of respiratory viruses, including low-pathogenic (LP) IAVs possessing a single arginine residue at the cleavage site. Here we show that TMPRSS2 plays an essential role in the proteolytic activation of LP IAVs, including a recently emerged H7N9 subtype, *in vivo*. We generated TMPRSS2 knockout (KO) mice. The TMPRSS2 KO mice showed normal reproduction, development, and growth phenotypes. In TMPRSS2 KO mice infected with LP IAVs, cleavage of HA was severely impaired, and consequently, the majority of LP IAV progeny particles failed to gain infectivity, while the viruses were fully activated proteolytically in TMPRSS2$^{+/+}$ wild-type (WT) mice. Accordingly, in contrast to WT mice, TMPRSS2 KO mice were highly tolerant of challenge infection by LP IAVs (H1N1, H3N2, and H7N9) with ≥1,000 50% lethal doses (LD_{50}) for WT mice. On the other hand, a high-pathogenic H5N1 subtype IAV possessing a multibasic cleavage site was successfully activated in the lungs of TMPRSS2 KO mice and killed these mice, as observed for WT mice. Our results demonstrate that recently emerged H7N9 as well as seasonal IAVs mainly use the specific protease TMPRSS2 for HA cleavage *in vivo* and, thus, that TMPRSS2 expression is essential for IAV replication *in vivo*.

IMPORTANCE

Influenza A virus (IAV) is a leading pathogen that infects and kills many humans every year. We clarified that the infectivity and pathogenicity of IAVs, including a recently emerged H7N9 subtype, are determined primarily by a host protease, TMPRSS2. Our data showed that TMPRSS2 is the key host protease that activates IAVs *in vivo* through proteolytic cleavage of their HA proteins. Hence, TMPRSS2 is a good target for the development of anti-IAV drugs. Such drugs could also be effective for many other respiratory viruses, including the recently emerged Middle East respiratory syndrome (MERS) coronavirus, because they are also activated by TMPRSS2 *in vitro*. Consequently, the present paper could have a large impact on the battle against respiratory virus infections and contribute greatly to human health.

Influenza A virus (IAV) is classified in the *Orthomyxoviridae* family and is a leading agent that affects and kills humans worldwide. IAV enters target cells via endocytosis, and virus-cell membrane fusion occurs at the late endosomes, thus releasing the viral genome to start virus replication. Membrane fusion is mediated by the hemagglutinin (HA) protein, which is synthesized as the inactive precursor HA_0 and cleaved by a host cell protease(s) to gain fusion activity. Proteolytic cleavage of HA_0 into the HA_1 and HA_2 subunits is essential for HA to express membrane fusion activity and, consequently, for IAV to acquire infectivity.

The HA of low-pathogenic (LP) IAVs, for which infection remains localized at respiratory and/or alimentary epithelial cells in birds and mammals, including humans, possesses a single arginine residue at the cleavage site. The HA of LP IAVs is thought to be cleaved and activated by a specific protease(s) present exclusively in these tissues. Trypsin, miniplasmin, tryptase Clara, mast cell tryptase, and type II transmembrane serine proteases (TTSPs) such as TMPRSS2, human airway trypsin-like protease (HAT), TMPRSS4, and matriptase have been shown to cleave the HA of LP IAVs at the single arginine residue (1, 2). Previous studies have also demonstrated HA subtype and strain specificities of TTSPs (3–6). On the other hand, the HA of high-pathogenic (HP) IAVs such as HP H5N1, which causes fatal systemic infections, contains multiple basic amino acids at the cleavage site (7–9). The HA of HP IAVs is cleaved by ubiquitous intracellular proteases such as furin and proprotein convertase 5/6, which are present in all cell types (1, 2). The concept of host protease-dependent tissue tro-

Received 11 December 2013 Accepted 27 February 2014
Published ahead of print 5 March 2014
Editor: T. S. Dermody
Address correspondence to Makoto Takeda, mtakeda@nih.go.jp.

doi:10.1128/JVI.03677-13

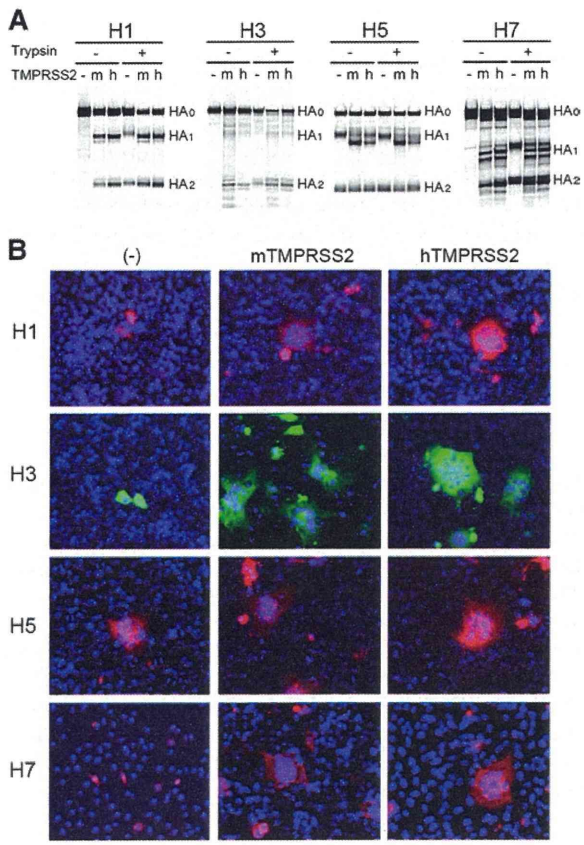

FIG 1 Proteolytic activation of HA by TMPRSS2. (A) HA proteins (H1, H3, H5, and H7 subtypes) were expressed alone (−) or together with mTMPRSS2 (m) or hTMPRSS2 (h) in 293T cells using expression plasmids. The cells were pulse labeled, and the HA components (HA_0, HA_1, and HA_2) were detected and analyzed by immunoprecipitation and SDS-PAGE. (B) HA proteins were expressed in HeLa/mTMPRSS2, HeLa/hTMPRSS2, or parental HeLa (−) cells. At 2 days posttransfection, the cells were treated with low-pH buffer (pH 5.3), and cell-cell fusion was analyzed by immunofluorescence staining using anti-IAV antibodies coupled with Alexa Fluor 488- or 549-conjugated secondary antibodies. The nuclear DNA was stained with DAPI.

pism and pathogenicity of LP and HP IAVs has been well established (7–9). However, the protease(s) directly involved in the cleavage activation of each HA subtype remains to be identified.

In the present study, we focused primarily on TMPRSS2 because this protease is expressed in the respiratory tract, activates a variety of respiratory viruses, and cleaves the HA of IAVs efficiently, even at marginal levels of expression, *in vitro* (4, 10–16). Our working hypothesis was that if TMPRSS2 is essential for IAV activation *in vivo*, mice lacking TMPRSS2 expression (TMPRSS2 knockout [KO] mice) are highly tolerant of challenge infection by IAVs that use primarily TMPRSS2 for HA cleavage.

MATERIALS AND METHODS

Ethics statement. All experiments with animals were performed in strict accordance with the animal experimentation guidelines of the National Institute of Infectious Diseases. The protocol was approved by the Institutional Animal Care and Use Committee of the institute (permit numbers 113066-II, 313008-II, and 13-09).

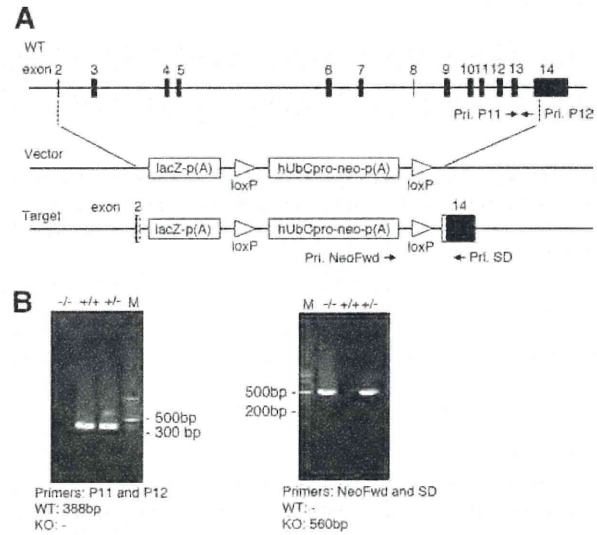

FIG 2 Structure of the targeted TMPRSS2 gene. (A) TMPRSS2 KO mice possess an allele [$Tmprss2^{tm1(KOMP)Vlcg}$] with an ablating deletion of the TMPRSS2 gene, which was replaced by the *lacZ* gene (VelociGene KOMP definitive null allele design). (B) The genotype was analyzed by VelociGene KOMP allele PCR genotyping strategies using primers NeoFwd and SD and a previously reported method using primers P11 and P12 (25).

TABLE 1 Transcriptome analysis of lungs from WT and TMPRSS2 KO mice for TTSPs

Gene	RPKM			
	Lungs		Bronchi	
	WT	KO	WT	KO
TTSPs				
Tmprss2	2.43	0.59[a]	3.62	0.51[a]
Tmprss3	0.00	0.00	0.21	0.00
Tmprss4	0.54	0.64	0.61	0.40
Tmprss5	0.05	0.21	1.61	0.38
Tmprss6	0.01	0.00	0.02	0.05
Tmprss7	0.39	0.00	0.01	0.03
Tmprss9	0.00	0.00	0.03	0.02
Tmprss11a	0.17	0.00	0.42	0.13
Tmprss11bnl	0.32	0.00	0.00	0.00
Tmprss11c	0.09	0.32	0.00	0.00
Tmprss11d	0.53	0.00	0.00	0.00
Tmprss11e	0.07	0.00	0.00	0.00
Tmprss11f	0.03	0.00	0.00	0.00
Tmprss11g	0.01	0.02	0.00	0.00
Tmprss12	0.00	0.00	0.00	0.00
Tmprss13	0.03	0.00	2.22	1.46
Tmprss15	0.01	0.02	0.11	0.07
Hpn	0.00	0.00	2.23	3.11
Lrp4	9.43	15.75	1.77	2.23
St14	0.35	4.35	12.96	13.74
Internal controls				
Gapdh	31.06	86.26	441.28	794.44
Actb	264.31	491.48	308.25	296.38

[a] Detected reads were mapped to exon 14 in the Tmprss2 coding sequence remaining in the TMPRSS2 KO mouse genome.

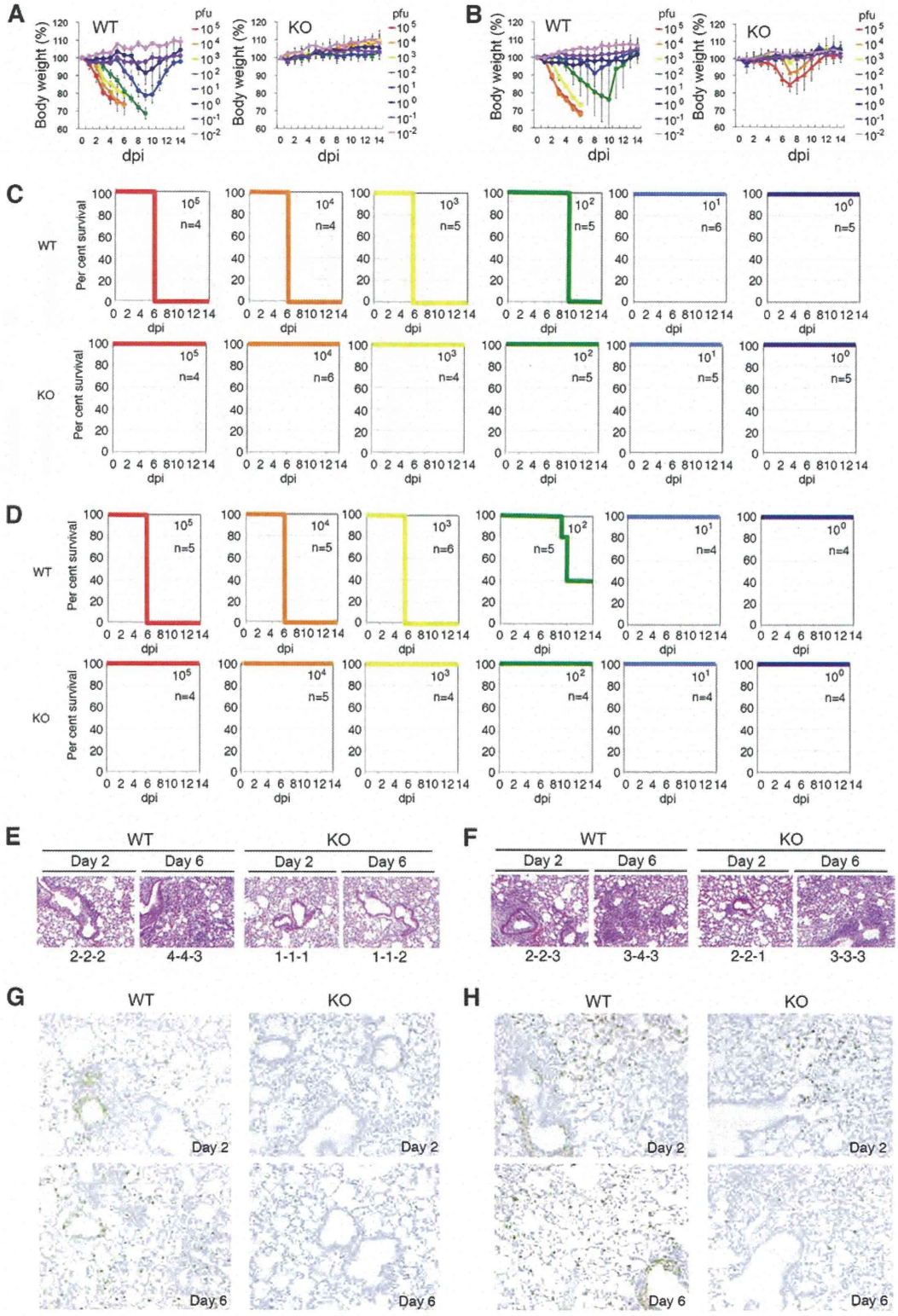

Plasmids. A mouse TMPRSS2 (mTMPRSS2) expression plasmid, pTarget-mTMPRSS2, was generated by inserting the mTMPRSS2 cDNA obtained from a C57BL/6 mouse. The human TMPRSS2 (hTMPRSS2) expression plasmid pcDNA-TMPRSS2 was reported previously (11). IAV HA expression plasmids pCAGGS-H1, -H3, -H5, and -H7 were generated by inserting cDNAs of the HA-coding region from mouse-adapted (MA) A/California/04/09 (MA-CA04[H1N1]) (17), MA-A/Guizhou-X (MA-GZX[H3N2]) (18), A/Vietnam/1194/04 (VN1194[H5N1]) (19), and A/Anhui/1/2013 (Anhui1[H7N9]) (20), respectively.

Cells and viruses. MDCK, HeLa, and 293T cells were cultured in Dulbecco's modified Eagle's medium (DMEM) supplemented with 5% fetal calf serum (FCS). HeLa cells were transfected with pTarget-mTMPRSS2 or pcDNA-TMPRSS2, and Geneticin-resistant stable clones (HeLa/mTMPRSS2 and HeLa/hTMPRSS2, respectively) were selected in the presence of 1.0 mg/ml of Geneticin (G418; Nacalai Tesque). MA-CA04[H1N1] was generated by reverse genetics as reported previously (17). MA-GZX[H3N2], VN1194[H5N1], and Anhui1[H7N9] were reported previously (18–20).

Structural modeling of hTMPRSS2 and mTMPRSS2. No known structures of mTMPRSS2 or hTMPRSS2 are available. Therefore, three-dimensional structural models of hTMPRSS2 and mTMPRSS2 were generated by a homology modeling method using several protease structures as the templates. The I-TASSER modeling server (21) was used for modeling. The X-ray structure most similar to both TMPRSS2 models was the human transmembrane serine protease hepsin (PDB accession number 1Z8G). The models were refined by energy minimization using Swiss-PdbViewer (22) and finally evaluated by PROCHECK (23) and Verify3D (24).

Cell fusion assay. HeLa/mTMPRSS2, HeLa/hTMPRSS2, and parental HeLa cells were transfected with an HA-expressing plasmid (pCAGGS-H1, -H3, -H5, or -H7) by using X-tremeGENE HP DNA transfection reagent (Roche). At 2 days posttransfection, the cells were washed with phosphate-buffered saline (PBS) and treated with prewarmed low-pH buffer (145 mM NaCl, 20 mM sodium citrate [pH 5.3]) for 2 min. The low-pH buffer was then replaced with DMEM–5% FCS, and the cells were incubated at 37°C for 3 h. Cell-cell fusion was analyzed by immunofluorescence staining using anti-IAV rabbit serum against H7, anti-IAV goat serum against H3, and HA-specific rabbit monoclonal antibodies (clone 327 for H1 and clone 89 for H5) coupled with Alexa Fluor 488- or 549-conjugated secondary antibodies. The nuclear DNA was stained with 4′,6′-diamidino-2-phenylindole (DAPI).

Pulse labeling and immunoprecipitation. Monolayers of 293T cells were transfected with an HA-expressing plasmid (pCAGGS-H1, -H3, -H5, or -H7) alone or together with a TMPRSS2-expressing plasmid (pTarget-mTMPRSS2 or pcDNA-TMPRSS2). At 20 h posttransfection, the cells were cultured in methionine-cysteine-deficient medium for 1 h and then pulse labeled with [^{35}S]methionine-cysteine by using EasyTag EXPRE35S35S protein labeling mix (PerkinElmer) for 1 h. The cells in some wells were treated with 1 μg/ml acetylated trypsin (Sigma) for 1 h, as a trypsin-activated HA control, and all cells were lysed in radioimmunoprecipitation assay (RIPA) buffer. Polypeptides in the cell lysates were immunoprecipitated with anti-IAV rabbit sera against H3 and H7 (Sino Biological Inc.) and HA-specific rabbit monoclonal antibodies (clone 327 for H1 and clone 89 for H5) and analyzed by SDS-PAGE.

Generation of TMPRSS2 KO mice. TMPRSS2 gene KO C57BL/6 embryonic stem (ES) cells (product number VG13341) were obtained from the Knockout Mouse Project (KOMP) Repository (UC Davis). The ES cells possessed an allele [Tmprss2$^{tm1(KOMP)Vlcg}$] with an ablating deletion of the TMPRSS2 gene, which was replaced by the *lacZ* gene (VelociGene KOMP definitive null allele design). The ES cells were injected into C57BL/6 mouse blastocysts, and chimeric mice in a complete C57BL/6 genetic background were generated. Male chimeric mice were selected by VelociGene KOMP allele PCR genotyping strategies by using primers NeoFwd and SD and a previously reported method using primers P11 and P12 (25) and mated with normal female C57BL/6 mice to generate C57BL/6 mice with a heterozygous genotype of the TMPRSS2 gene (TMPRSS2$^{+/-}$). TMPRSS2 KO mice with a homologous genotype (TMPRSS2$^{-/-}$) were obtained by crossing male and female TMPRSS2$^{+/-}$ C57BL/6 mice.

Transcriptome analysis. The bronchi and right middle lobes of the lung were obtained from uninfected healthy wild-type (WT) and KO (TMPRSS2$^{-/-}$) mice (6-week-old females). Total RNA was prepared from ~50 mg of the bronchi or right middle lobes treated with RNAlater (Life Technologies), using a RecoverAll Total Nucleic Acid Isolation kit (Ambion), followed by selection of poly(A) mRNA using a FastTrack

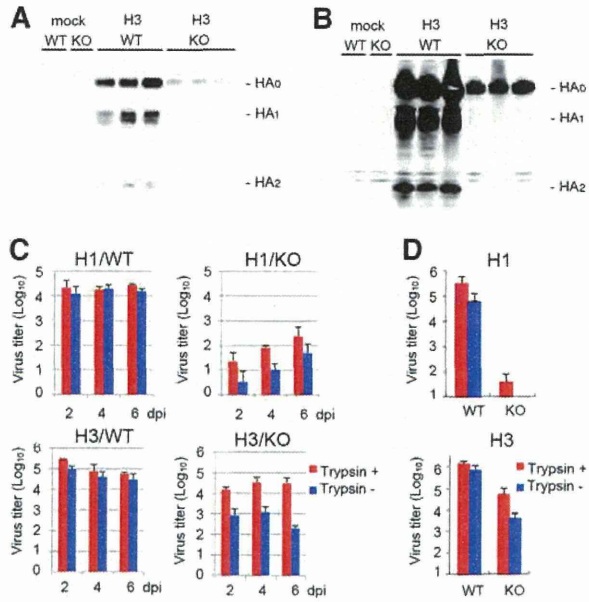

FIG 4 Proteolytic activation of IAVs *in vivo*. (A and B) WT and TMPRSS2 KO mice were intranasally inoculated with PBS (mock) (n = 1) or MA-GZX[H3N2] (n = 3). Lung lavage fluids (A) and lung homogenates (B) were collected at 6 dpi, and HA was analyzed by SDS-PAGE and immunoblotting. Each lane corresponds to data from an individual mouse. (C and D) WT and TMPRSS2 KO mice were intranasally inoculated with MA-CA04[H1N1] (n = 3) or MA-GZX[H3N2] (n = 3). Lung lavage fluids at 2, 4, and 6 dpi (C) and lung homogenates at 2 dpi (D) were either untreated (Trypsin −) or treated with trypsin (Trypsin +) and used for virus titration. Error bars represent standard deviations.

FIG 3 Role of TMPRSS2 in H1N1 and H3N2 IAV pathogenicity. (A and B) WT and TMPRSS2 KO mice were intranasally inoculated with different doses of MA-CA04[H1N1] (A) or MA-GZX[H3N2] (B) (n = 4 to 7). Body weights were measured daily. Error bars represent standard deviations. (C and D) Survival curves of IAV-infected mice. WT and TMPRSS2 KO mice were challenged with different doses of MA-CA04[H1N1] (C) or MA-GZX[H3N2] (D). For each experimental group, 4 to 6 mice were used. (E to H) Histopathological findings in the lungs of WT and TMPRSS2 KO mice infected with MA-CA04[H1N1] (E and G) or MA-GZX[H3N2] (F and H). Data obtained by hematoxylin and eosin staining (magnification, ×10) (E and F) and immunohistochemistry for the IAV nucleocapsid protein (magnification, ×10) (G and H) are shown. The inflammation scores of individual mice (n = 3) are shown at the bottom of each panel (E and F): 0, no apparent changes; 1, minimal changes or bronchiolitis; 2, bronchiolitis and/or slight alveolitis; 3, mild alveolitis with neutrophils, monocytes/macrophages, or lymphocytes; 4, moderate alveolitis.

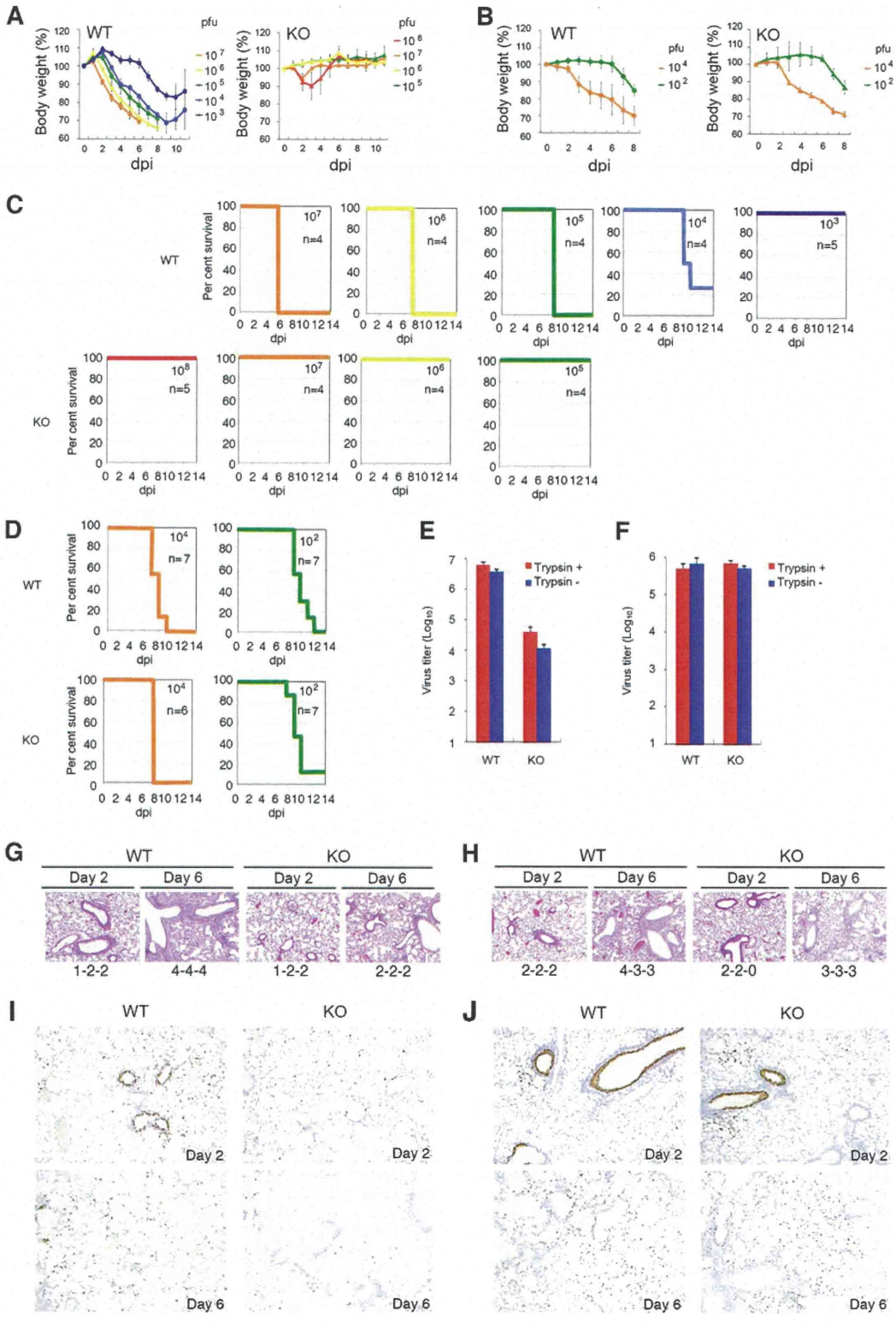

MAG mRNA isolation kit (Invitrogen). RNA strand-specific transcriptome sequencing (RNA-seq) libraries were prepared from ~50 ng of the purified poly(A) mRNA using a ScriptSeq v2 RNA-Seq Library Preparation kit (Epicentre). The prepared RNA-seq library was sequenced by using a GAIIx sequencer (Illumina). The obtained strand-specific short reads were analyzed by CLC Genome Workbench (v. 6.05) with mean expression normalization against *Mus musculus* reference genome sequences (GRCm38.p1), and genes showing significant differential expression were detected with a false discovery rate (FDR) of <0.05 and changes of ≥2-fold. The reads per kilobase of exon model per million mapped reads (RPKM) were estimated for each transcriptome experiment.

Titration of infectious units. To determine the infectious virus titers activated *in vivo*, monolayers of MDCK cells in 12-well plates were infected with serially diluted virus samples for 1 h at 4°C, washed twice with PBS, overlaid with DMEM–1% agarose, and incubated for 24 h at 37°C to allow the viruses to enter the cells. Trypsin was omitted to avoid HA cleavage before virus entry. At 24 h postinfection, the cell monolayers were additionally overlaid with DMEM–1% agarose supplemented with 2.0 μg/ml of trypsin to allow plaque formation. The virus titers obtained with this method were essentially equivalent to those obtained by immunofluorescence staining techniques (26), in which trypsin was omitted during the entire process of titration and individual infected cells, instead of plaques, were detected and counted. To determine the infectious titers of viruses that had not been activated *in vivo* but possessed infectious potential, virus samples were treated with 1.0 μg/ml of trypsin and subjected to a standard plaque assay.

Infection of mice. KO (TMPRSS2$^{-/-}$) and WT (TMPRSS2$^{+/+}$) C57BL/6 mice (6- to 7-week-old males or females) were challenged with MA-CA04[H1N1], MA-GZX[H3N2], VN1194[H5N1], or Anhui1 [H7N9]. For each mouse, 20 μl of virus solution containing different amounts of IAV was inoculated intranasally. For mock infection, the same volume of PBS was used. For each experimental group, 4 to 6 mice were used to monitor body weight. To analyze the *in vivo* activation and replication of IAV, WT and TMPRSS2 KO mice were challenged with 4.0×10^3 PFU of MA-CA04[H1N1] or 6.8×10^3 PFU of MA-GZX[H3N2]. Lung lavage fluids collected at 2, 4, and 6 days postinfection (dpi) and lung homogenates collected at 2 dpi were either untreated or treated with trypsin to determine the virus titers activated *in vivo* and *in vitro*, respectively. Three mice were used for each experimental group, and samples were collected separately from individual mice. For histopathological examinations, WT and TMPRSS2 KO mice were infected with 4.0×10^3 PFU (3.0×10^2 50% lethal doses [LD_{50}]) of MA-CA04[H1N1], 6.8×10^3 PFU (1.0×10^2 LD_{50}) of MA-GZX[H3N2], 1.0×10^4 PFU (1.0×10^2 LD_{50}) of VN1194[H5N1], or 4.0×10^6 PFU (1.0×10^2 LD_{50}) of Anhui1[H7N9]; euthanized; and autopsied at 2 and 6 dpi. Three mice were used for each experimental group.

Immunoblotting. The lung lavage fluids and lung homogenates were mixed with lysis buffer to make a final solution containing 150 mM NaCl, 50 mM Tris-HCl (pH 7.5), 4 mM EDTA, 0.1% sodium deoxycholate, 1% Nonidet P-40, and 0.1% SDS, containing a complete protease inhibitor mixture (Roche Diagnostics). The polypeptides were then separated by SDS-PAGE and immunoblotted. A rabbit antiserum raised against H3 (Sino Biological Inc.) was used for detection.

Nucleotide sequence accession number. The RNA-seq reads of the lung tissues from WT and TMPRSS2 KO mice are available at the DDBJ Sequence Read Archive under accession number DRA001103 (47,935,571 and 46,863,938 paired-end reads for WT and TMPRSS2 KO mice, respectively).

RESULTS

mTMPRSS2 proteolytically activates IAV HAs similarly to hTMPRSS2. To obtain a biological rationale for performing mouse experiments, we analyzed mTMPRSS2. Three-dimensional structural models of mTMPRSS2 and hTMPRSS2 showed strong conservation of amino acid residues near the protease active site (data not shown). Based on the strong homology between hTMPRSS2 and mTMPRSS2, these proteases were strongly suggested to have similar substrate specificities. However, the TMPRSS2 structures were strictly models, and biological analyses were performed. The analyses showed that all HAs of LP IAVs of the H1, H3, and H7 subtypes were cleaved by both mTMPRSS2 and hTMPRSS2 (Fig. 1A), and the cleaved HAs showed cell-cell fusion (syncytium formation) activity (Fig. 1B). As expected, cleavage and activation of HA of an HP IAV of the H5 subtype occurred independently of TMPRSS2 expression (Fig. 1A and B). Consistent with previous data (27), different molecular sizes of HA were detected in TMPRSS2-expressing cells, because the expression of TMPRSS2 modulates the HA glycosylation pattern (Fig. 1A).

TMPRSS2 is essential for the pathogenicity of H1N1 and H3N2 IAVs. TMPRSS2 KO mice, which possessed an ablating deletion including exons 3 to 13 of the TMPRSS2 gene, were generated in a complete C57BL/6 genetic background (Fig. 2). To confirm whether TMPRSS2 KO induced unexpected differential expression of other TTSPs, RNA-seq experiments were performed. The transcriptome analysis indicated that TMPRSS2 KO did not significantly affect the expressions of other TTSP genes and potential protease genes (Table 1). As an exception, the level of St14 appeared to be increased in the TMPRSS2 KO mouse lung (Table 1), but the raw count was still very low, and the change was judged to be insignificant based on the FDR analysis. However, our data did not exclude the possibility that the change was induced by TMPRSS2 gene KO. TMPRSS2 KO mice exhibited normal reproduction, development, and growth patterns, similarly to WT C57BL/6 mice, as observed for previously reported TMPRSS2 KO mice with a deletion of exons 10 to 13 in the TMPRSS2 gene (25).

Various doses of MA viruses of human LP IAV strains MA-CA04[H1N1] and MA-GZX[H3N2] were inoculated intranasally into WT and TMPRSS2 KO mice. All WT mice inoculated with ≥10^2 PFU (7.5 LD_{50}) of MA-CA04[H1N1] died or required euthanasia (Fig. 3A and C). In strong contrast, TMPRSS2 KO mice challenged with up to 10^5 PFU (7.5×10^3 LD_{50}) showed neither clinical signs nor body weight loss (Fig. 3A and C). TMPRSS2 KO mice were also highly tolerant of lethal challenge infections with MA-

FIG 5 Role of TMPRSS2 in H5N1 and H7N9 IAV pathogenicity. (A and B) WT and TMPRSS2 KO mice were intranasally inoculated with different doses of Anhui1[H7N9] (A) or VN1194[H5N1] (B) ($n = 4$ to 6). The body weights were measured daily. Error bars represent standard deviations. (C and D) Survival curves of IAV-infected mice. WT and TMPRSS2 KO mice were challenged with different doses of Anhui1[H7N9] (C) or VN1194[H5N1] (D). For each experimental group, 4 to 7 mice were used. (E and F) WT and TMPRSS2 KO mice were intranasally inoculated with Anhui1[H7N9] ($n = 3$) or VN1194[H5N1] ($n = 3$). Lung homogenates at 4 dpi (D) were either untreated (Trypsin −) or treated with trypsin (Trypsin +) and used for virus titration. Error bars represent standard deviations. (G to J) Histopathological findings in the lungs of WT and TMPRSS2 KO mice infected with Anhui1[H7N9] (G and I) or VN1194[H5N1] (H and J). Data obtained by hematoxylin and eosin staining (magnification, ×10) (G and H) and immunohistochemistry for the IAV nucleocapsid protein (magnification, ×10) (I and J) are shown. The inflammation scores of individual mice ($n = 3$) are shown at the bottom of each panel (G and H): 0, no apparent changes; 1, minimal changes or bronchiolitis; 2, bronchiolitis and/or slight alveolitis; 3, mild alveolitis with neutrophils, monocytes/macrophages, or lymphocytes; 4, moderate alveolitis.

GZX[H3N2] (Fig. 3B and D). All TMPRSS2 KO mice infected with 10^5 PFU (1.5×10^3 LD_{50}) of MA-GZX[H3N2] showed moderate body weight loss but recovered completely (Fig. 3B and D).

Figure 3E to H shows the histopathology of lungs of mice infected with 4.0×10^3 PFU (3.0×10^2 LD_{50}) of MA-CA04[H1N1] or 6.8×10^3 PFU (1.0×10^2 LD_{50}) of MA-GZX[H3N2]. WT mice infected with each virus developed bronchiolitis and peribronchial inflammation, with a few foci of alveolitis at 2 dpi and mild to moderate alveolitis at 6 dpi (Fig. 3E and F). Viral antigens were detected in bronchial epithelial cells and alveolar lining cells in the lungs of WT mice at 2 dpi and had spread dramatically to the entire lungs by 6 dpi (Fig. 3G and H). In contrast, the lungs of KO mice infected with the same viruses exhibited significantly reduced levels of inflammation (Fig. 3E and F). Viral antigen-positive cells did not spread during the observation period (Fig. 3G and H). Viral antigens were almost completely eliminated from bronchiolar epithelial cells of KO mice by 6 dpi (Fig. 3G and H).

TMPRSS2 is essential for proteolytic activation of IAVs *in vivo*. To explore the cleavage of HA in the lungs, WT and TMPRSS2 KO mice were infected with 4.0×10^3 PFU (3.0×10^2 LD_{50}) of MA-CA04[H1N1] or 6.8×10^3 PFU (1.0×10^2 LD_{50}) of MA-GZX[H3N2]. At 6 dpi, lung lavage fluids were collected from mice infected with MA-GZX[H3N2] and analyzed for HA protein by SDS-PAGE and immunoblotting. Cleavage of HA was demonstrated in WT mice, as signals for the HA_1 and HA_2 subunits were clearly detected in these mice (Fig. 4A). In contrast, only the HA_0 precursor was detected in TMPRSS2 KO mice, and HA_1 and HA_2 remained undetectable (Fig. 4A). Similarly, lung homogenates of the infected mice were analyzed. HA was efficiently cleaved into HA_1 and HA_2 in the lung homogenates of WT mice (Fig. 4B). Meanwhile, the lung homogenates of TMPRSS2 KO mice showed HA_0 signals, but HA_1 and HA_2 were undetectable (Fig. 4B). These findings indicated that the HA protein of progeny viruses present in the respiratory tract had been cleaved in WT mice, while HA cleavage was severely impaired in TMPRSS2 KO mice. To verify whether the infectivity of the progeny viruses from each mouse lung was activated *in vivo*, lung lavage fluids at 2, 4, and 6 dpi and lung homogenates at 2 dpi were treated or untreated with trypsin *in vitro* and compared for infectivity *in vitro* to determine virus titers. At 2 dpi, the virus titers of MA-CA04[H1N1] and MA-GZX[H3N2] reached their peak levels in WT mice (Fig. 4C). The HAs of progeny viruses were shown to be fully activated in WT mice, since the virus infectivity titers without trypsin treatment (Fig. 4C and D) were similar to those after activation *in vitro* (Fig. 4C and D). The virus titers in the lungs of TMPRSS2 KO mice were much lower than those in the lungs of WT mice (Fig. 4C and D), showing restricted virus growth in TMPRSS2 KO mice. Importantly, the virus titers (Fig. 4C and D) were further increased 10 to 100 times after trypsin treatment *in vitro* (Fig. 4C and D). These data demonstrated that the great majority (90 to 99%) of the progeny virus particles failed to be proteolytically activated in TMPRSS2 KO mice.

TMPRSS2 is essential for LP H7N9 IAV, but dispensable for HP H5N1 IAV, to exhibit pathogenicity. The pathogenicity of a human isolate of an emerging LP H7N9 subtype virus, Anhui1 [H7N9], was also analyzed. Anhui1[H7N9] was inoculated intranasally into WT and TMPRSS2 KO mice. As shown in Fig. 5A and C, TMPRSS2 KO mice were highly tolerant of H7N9 virus infection. All WT mice infected with 10^5 PFU (5.0×10 LD_{50}) of Anhui1[H7N9] died or required euthanasia by 8 dpi (Fig. 5A and C). In contrast, all TMPRSS2 KO mice infected with the same dose (10^5 PFU [5.0×10 LD_{50}]) showed no clinical signs, and those infected with a 1,000-times-higher dose, 10^8 PFU (5.0×10^4 LD_{50}), showed only temporary and mild body weight loss (Fig. 5A). The virus titers in the KO mouse lungs were much lower than those in the WT mouse lungs (Fig. 5E). Histopathological examinations of mouse lungs infected with 4.0×10^6 PFU of Anhui1[H7N9] showed that Anhui1[H7N9] spread poorly in the lungs of TMPRSS2 KO mice (Fig. 5G and I).

In contrast to the findings for the LP IAVs described above, a human isolate of an HP H5N1 subtype virus, VN1194[H5N1], caused severe body weight loss, neurological symptoms, and death or requirement for euthanasia by 8 or 9 dpi in both WT and TMPRSS2 KO mice infected with 10^4 PFU (2.0×10^3 LD_{50}) of VN1194[H5N1] (Fig. 5B and D). The survival curves of WT and TMPRSS2 KO mice infected with 10^2 PFU (5.0×10 LD_{50}) of VN1194[H5N1] were also similar to one another (Fig. 5B and D). The virus titers in the lungs were equivalent between WT and KO mice (Fig. 5F). Histopathological examinations of mouse lungs infected with 1.0×10^4 PFU of VN1194[H5N1] demonstrated that VN1194[H5N1] spread efficiently in a similar manner in the lungs of WT and TMPRSS2 KO mice (Fig. 5H and J). The overall results indicated that, unlike LP IAVs, proteolytic activation of the HP H5N1 virus occurred in mouse lungs independently of TMPRSS2.

DISCUSSION

In the last decade, we have experienced outbreaks of a swine-origin LP H1N1 IAV and the severe acute respiratory syndrome (SARS) coronavirus (28, 29). These outbreaks proved that respiratory viruses can currently spread rapidly and that the available strategies are insufficiently effective to prevent global transmission of emerging respiratory viruses (28). At this time, H5N1 and H7N9 IAVs and the Middle East respiratory syndrome (MERS) coronavirus are potential threats for humans (29, 30).

The present study has provided concrete evidence that TMPRSS2 expression is essential for *in vivo* replication of emerging H7N9 and seasonal IAVs and that this protease primarily determines IAV pathogenicity. Based on the strong homology between hTMPRSS2 and mTMPRSS2, hTMPRSS2 is strongly suggested to play a similar role in the activation and pathogenicity of human IAVs *in vivo*. In human airway bronchial epithelial cells, TMPRSS2 is expressed by type 1 and type 2 pneumocytes of the alveolar epithelium and alveolar macrophages (12, 31). In the airway, IAV particles are released exclusively from the apical membrane (32). To achieve this, the IAV HA protein is specifically targeted to the apical plasma membrane (33, 34), and TMPRSS2 is selectively expressed at the apical membrane of airway epithelial cells (35). Taking these data into consideration, it is most likely that LP IAVs use primarily the specific host protease TMPRSS2 for HA activation in the lungs. However, our data do not exclude the possibility that TMPRSS2 may activate a precursor of another protease(s) that finally induces HA activation. Nevertheless, our data showing the critical role of TMPRSS2 expressed in the respiratory tract in the activation of IAV pathogenicity *in vivo* support the concept of host protease-mediated pathogenicity of IAVs (7–9).

The present findings suggest that TMPRSS2 is a good target for the development of anti-LP IAV drugs. The membrane-anchoring and cytoplasmic domains of TTSPs regulate cellular trafficking

and localization of TTSPs, thereby enabling temporal and spatial regulation of substrate processing (36–38). Accordingly, by targeting specific substrates such as peptide hormones, growth factors, differentiation factors, receptors, and adhesion molecules, TTSPs play a variety of critical roles in developmental stages and physiological events (36–38). A previous study suggested that TMPRSS2 regulates Na^+ currents (39). However, the physiological roles of TMPRSS2 remain to be elucidated (40), because TMPRSS2 KO mice showed a normal phenotype.

During the submission process for the present paper, Hatesuer et al. (41) reported a similar study demonstrating a critical role of TMPRSS2 in the pathogenicity of H1N1 and H3N2 IAVs in mice. They used a previously reported TMPRSS2 KO mouse strain with a deletion of exons 10 to 13 in the TMPRSS2 gene (25, 41). The TMPRSS2 KO mice with a deletion of exons 3 to 13 in the TMPRSS2 gene established in the present study exhibited phenotypes very similar to those of their mice, providing a very strong conclusion that TMPRSS2 expression is essential for IAV pathogenesis. Interestingly, in agreement with their data (41), our study demonstrated that replication of H1N1 IAV was more severely restricted in TMPRSS2 KO mice than that of H3N2 IAV. Therefore, cleavage of the H1 subtype appears to be more strongly dependent on TMPRSS2 expression than cleavage of the H3 subtype.

Finally, TTSPs have a clear substrate specificity (37). Nevertheless, various respiratory viruses, including the SARS coronavirus (12, 42–44), MERS coronavirus (14), human metapneumovirus (11), and parainfluenza viruses (13), also use TMPRSS2 for their activation. These observations imply that a variety of respiratory viruses may specifically exploit TMPRSS2 for activation. Drugs that inhibit TMPRSS2 are therefore expected to be effective against a wide spectrum of respiratory viruses. Meanwhile, different types of drugs targeting ubiquitous proteases other than TMPRSS2 may be required for HP IAVs such as the H5N1 virus subtype.

ACKNOWLEDGMENTS

The ES cells used for this research project were generated by the Trans-NIH Knockout Mouse Project (KOMP) and obtained from the KOMP Repository (http://www.komp.org/). NIH grants to VelociGene at Regeneron Inc. (U01HG004085) and the CSD Consortium (U01HG004080) funded the generation of gene-targeted ES cells for 8,500 genes in the KOMP Program, which were archived and distributed by the KOMP Repository at UC Davis and CHORI (U42RR024244). This work was supported by grants-in-aid from the Ministry of Education, Science, Sports and Culture of Japan (KAKENHI; 23390114), the Takeda Science Foundation, and ERATO, Japan, and by a National Institute of Allergy and Infectious Diseases Public Health Service research grant.

We thank Yuelong Shu, Chinese Center for Disease Control and Prevention, and Le Quynh Mai, National Institute of Hygiene and Epidemiology, for providing H7N9 IAV and H5N1 IAV, respectively; R. A. Lamb, Northwestern University, for providing anti-IAV serum; and E. Takashita, M. Shirakura, H. Asanuma, H. Fukuhara, A. Sato, N. Nagata, Y. Sato, and all our members in the Department of Virology 3, NIID, for suggestions and technical support.

REFERENCES

1. **Kido H, Okumura Y, Takahashi E, Pan HY, Wang S, Yao D, Yao M, Chida J, Yano M.** 2012. *Role of host cellular proteases in the pathogenesis of influenza and influenza-induced multiple organ failure.* Biochim. Biophys. Acta **1824:**186–194. http://dx.doi.org/10.1016/j.bbapap.2011.07.001.
2. **Bottcher-Friebertshauser E, Klenk HD, Garten W.** 2013. Activation of influenza viruses by proteases from host cells and bacteria in the human airway epithelium. Pathog. Dis. **69:**87–100. http://dx.doi.org/10.1111/2049-632X.12053.
3. **Beaulieu A, Gravel E, Cloutier A, Marois I, Colombo E, Desilets A, Verreault C, Leduc R, Marsault E, Richter MV.** 2013. Matriptase proteolytically activates influenza virus and promotes multicycle replication in the human airway epithelium. J. Virol. **87:**4237–4251. http://dx.doi.org/10.1128/JVI.03005-12.
4. **Baron J, Tarnow C, Mayoli-Nussle D, Schilling E, Meyer D, Hammami M, Schwalm F, Steinmetzer T, Guan Y, Garten W, Klenk HD, Bottcher-Friebertshauser E.** 2013. Matriptase, HAT, and TMPRSS2 activate the hemagglutinin of H9N2 influenza A viruses. J. Virol. **87:**1811–1820. http://dx.doi.org/10.1128/JVI.02320-12.
5. **Galloway SE, Reed ML, Russell CJ, Steinhauer DA.** 2013. Influenza HA subtypes demonstrate divergent phenotypes for cleavage activation and pH of fusion: implications for host range and adaptation. PLoS Pathog. **9:**e1003151. http://dx.doi.org/10.1371/journal.ppat.1003151.
6. **Hamilton BS, Gludish DW, Whittaker GR.** 2012. Cleavage activation of the human-adapted influenza virus subtypes by matriptase reveals both subtype and strain specificities. J. Virol. **86:**10579–10586. http://dx.doi.org/10.1128/JVI.00306-12.
7. **Bosch FX, Garten W, Klenk HD, Rott R.** 1981. Proteolytic cleavage of influenza virus hemagglutinins: primary structure of the connecting peptide between HA1 and HA2 determines proteolytic cleavability and pathogenicity of avian influenza viruses. Virology **113:**725–735. http://dx.doi.org/10.1016/0042-6822(81)90201-4.
8. **Kawaoka Y, Webster RG.** 1988. Sequence requirements for cleavage activation of influenza virus hemagglutinin expressed in mammalian cells. Proc. Natl. Acad. Sci. U. S. A. **85:**324–328. http://dx.doi.org/10.1073/pnas.85.2.324.
9. **Rott R, Klenk HD, Nagai Y, Tashiro M.** 1995. Influenza viruses, cell enzymes, and pathogenicity. Am. J. Respir. Crit. Care Med. **152:**S16–S19. http://dx.doi.org/10.1164/ajrccm/152.4_Pt_2.S16.
10. **Bottcher E, Matrosovich T, Beyerle M, Klenk HD, Garten W, Matrosovich M.** 2006. Proteolytic activation of influenza viruses by serine proteases TMPRSS2 and HAT from human airway epithelium. J. Virol. **80:**9896–9898. http://dx.doi.org/10.1128/JVI.01118-06.
11. **Shirogane Y, Takeda M, Iwasaki M, Ishiguro N, Takeuchi H, Nakatsu Y, Tahara M, Kikuta H, Yanagi Y.** 2008. Efficient multiplication of human metapneumovirus in Vero cells expressing the transmembrane serine protease TMPRSS2. J. Virol. **82:**8942–8946. http://dx.doi.org/10.1128/JVI.00676-08.
12. **Matsuyama S, Nagata N, Shirato K, Kawase M, Takeda M, Taguchi F.** 2010. Efficient activation of the severe acute respiratory syndrome coronavirus spike protein by the transmembrane protease TMPRSS2. J. Virol. **84:**12658–12664. http://dx.doi.org/10.1128/JVI.01542-10.
13. **Abe M, Tahara M, Sakai K, Yamaguchi H, Kanou K, Shirato K, Kawase M, Noda M, Kimura H, Matsuyama S, Fukuhara H, Mizuta K, Maenaka K, Ami Y, Esumi M, Kato A, Takeda M.** 2013. TMPRSS2 is an activating protease for respiratory parainfluenza viruses. J. Virol. **87:**11930–11935. http://dx.doi.org/10.1128/JVI.01490-13.
14. **Shirato K, Kawase M, Matsuyama S.** 2013. Middle East respiratory syndrome coronavirus (MERS-CoV) infection mediated by the transmembrane serine protease TMPRSS2. J. Virol. **87:**12552–12561. http://dx.doi.org/10.1128/JVI.01890-13.
15. **Gierer S, Bertram S, Kaup F, Wrensch F, Heurich A, Kramer-Kuhl A, Welsch K, Winkler M, Meyer B, Drosten C, Dittmer U, von Hahn T, Simmons G, Hofmann H, Pohlmann S.** 2013. The spike protein of the emerging betacoronavirus EMC uses a novel coronavirus receptor for entry, can be activated by TMPRSS2, and is targeted by neutralizing antibodies. J. Virol. **87:**5502–5511. http://dx.doi.org/10.1128/JVI.00128-13.
16. **Bertram S, Dijkman R, Habjan M, Heurich A, Gierer S, Glowacka I, Welsch K, Winkler M, Schneider H, Hofmann-Winkler H, Thiel V, Pohlmann S.** 2013. TMPRSS2 activates the human coronavirus 229E for cathepsin-independent host cell entry and is expressed in viral target cells in the respiratory epithelium. J. Virol. **87:**6150–6160. http://dx.doi.org/10.1128/JVI.03372-12.
17. **Sakabe S, Ozawa M, Takano R, Iwastuki-Horimoto K, Kawaoka Y.** 2011. *Mutations in PA, NP, and HA of a pandemic (H1N1) 2009 influenza* virus contribute to its adaptation to mice. Virus Res. **158:**124–129. http://dx.doi.org/10.1016/j.virusres.2011.03.022.
18. **Yoshikawa T, Matsuo K, Matsuo K, Suzuki Y, Nomoto A, Tamura S, Kurata T, Sata T.** 2004. Total viral genome copies and virus-Ig complexes

after infection with influenza virus in the nasal secretions of immunized mice. J. Gen. Virol. 85:2339–2346. http://dx.doi.org/10.1099/vir.0.79892-0.
19. Gao P, Watanabe S, Ito T, Goto H, Wells K, McGregor M, Cooley AJ, Kawaoka Y. 1999. Biological heterogeneity, including systemic replication in mice, of H5N1 influenza A virus isolates from humans in Hong Kong. J. Virol. 73:3184–3189.
20. Watanabe T, Kiso M, Fukuyama S, Nakajima N, Imai M, Yamada S, Murakami S, Yamayoshi S, Iwatsuki-Horimoto K, Sakoda Y, Takashita E, McBride R, Noda T, Hatta M, Imai H, Zhao D, Kishida N, Shirakura M, de Vries RP, Shichinohe S, Okamatsu M, Tamura T, Tomita Y, Fujimoto N, Goto K, Katsura H, Kawakami E, Ishikawa I, Watanabe S, Ito M, Sakai-Tagawa Y, Sugita Y, Uraki R, Yamaji R, Eisfeld AJ, Zhong G, Fan S, Ping J, Maher EA, Hanson A, Uchida Y, Saito T, Ozawa M, Neumann G, Kida H, Odagiri T, Paulson JC, Hasegawa H, Tashiro M, Kawaoka Y. 2013. Characterization of H7N9 influenza A viruses isolated from humans. Nature 501:551–555. http://dx.doi.org/10.1038/nature12392.
21. Roy A, Kucukural A, Zhang Y. 2010. I-TASSER: a unified platform for automated protein structure and function prediction. Nat. Protoc. 5:725–738. http://dx.doi.org/10.1038/nprot.2010.5.
22. Guex N, Peitsch MC. 1997. SWISS-MODEL and the Swiss-PdbViewer: an environment for comparative protein modeling. Electrophoresis 18:2714–2723. http://dx.doi.org/10.1002/elps.1150181505.
23. Laskowski RA, MacArthur MW, Moss DS, Thornton MJ. 1993. PROCHECK: a program to check the stereochemistry of protein structures. J. Appl. Crystallogr. 26:283–291. http://dx.doi.org/10.1107/S0021889892009944.
24. Eisenberg D, Luthy R, Bowie JU. 1997. VERIFY3D: assessment of protein models with three-dimensional profiles. Methods Enzymol. 277:396–404. http://dx.doi.org/10.1016/S0076-6879(97)77022-8.
25. Kim TS, Heinlein C, Hackman RC, Nelson PS. 2006. Phenotypic analysis of mice lacking the Tmprss2-encoded protease. Mol. Cell. Biol. 26:965–975. http://dx.doi.org/10.1128/MCB.26.3.965-975.2006.
26. Tashiro M, Ciborowski P, Klenk HD, Pulverer G, Rott R. 1987. Role of Staphylococcus protease in the development of influenza pneumonia. Nature 325:536–537. http://dx.doi.org/10.1038/325536a0.
27. Bertram S, Glowacka I, Blazejewska P, Soilleux E, Allen P, Danisch S, Steffen I, Choi SY, Park Y, Schneider H, Schughart K, Pohlmann S. 2010. TMPRSS2 and TMPRSS4 facilitate trypsin-independent spread of influenza virus in Caco-2 cells. J. Virol. 84:10016–10025. http://dx.doi.org/10.1128/JVI.00239-10.
28. Waterer G. 2011. Controlling epidemic viral infection. Curr. Opin. Infect. Dis. 24:130–136. http://dx.doi.org/10.1097/QCO.0b013e328343b720.
29. Graham RL, Donaldson EF, Baric RS. 2013. A decade after SARS: strategies for controlling emerging coronaviruses. Nat. Rev. Microbiol. 11:836–848. http://dx.doi.org/10.1038/nrmicro3143.
30. Cowling BJ, Jin L, Lau EH, Liao Q, Wu P, Jiang H, Tsang TK, Zheng J, Fang VJ, Chang Z, Ni MY, Zhang Q, Ip DK, Yu J, Li Y, Wang L, Tu W, Meng L, Wu JT, Luo H, Li Q, Shu Y, Li Z, Feng Z, Yang W, Wang Y, Leung GM, Yu H. 2013. Comparative epidemiology of human infections with avian influenza A H7N9 and H5N1 viruses in China: a population-based study of laboratory-confirmed cases. Lancet 382:129–137. http://dx.doi.org/10.1016/S0140-6736(13)61171-X.
31. Bertram S, Heurich A, Lavender H, Gierer S, Danisch S, Perin P, Lucas JM, Nelson PS, Pohlmann S, Soilleux EJ. 2012. Influenza and SARS-coronavirus activating proteases TMPRSS2 and HAT are expressed at multiple sites in human respiratory and gastrointestinal tracts. PLoS One 7:e35876. http://dx.doi.org/10.1371/journal.pone.0035876.
32. Rodriguez Boulan E, Sabatini DD. 1978. Asymmetric budding of viruses in epithelial monlayers [*sic*]: a model system for study of epithelial polarity. Proc. Natl. Acad. Sci. U. S. A. 75:5071–5075. http://dx.doi.org/10.1073/pnas.75.10.5071.
33. Nayak DP, Barman S. 2002. Role of lipid rafts in virus assembly and budding. Adv. Virus Res. 58:1–28. http://dx.doi.org/10.1016/S0065-3527(02)58001-5.
34. Takeda M, Leser GP, Russell CJ, Lamb RA. 2003. Influenza virus hemagglutinin concentrates in lipid raft microdomains for efficient viral fusion. Proc. Natl. Acad. Sci. U. S. A. 100:14610–14617. http://dx.doi.org/10.1073/pnas.2235620100.
35. Jacquinet E, Rao NV, Rao GV, Hoidal JR. 2000. Cloning, genomic organization, chromosomal assignment and expression of a novel mosaic serine proteinase: epitheliasin. FEBS Lett. 468:93–100. http://dx.doi.org/10.1016/S0014-5793(00)01196-0.
36. Hooper JD, Clements JA, Quigley JP, Antalis TM. 2001. Type II transmembrane serine proteases. Insights into an emerging class of cell surface proteolytic enzymes. J. Biol. Chem. 276:857–860. http://dx.doi.org/10.1074/jbc.R000020200.
37. Antalis TM, Buzza MS, Hodge KM, Hooper JD, Netzel-Arnett S. 2010. The cutting edge: membrane-anchored serine protease activities in the pericellular microenvironment. Biochem. J. 428:325–346. http://dx.doi.org/10.1042/BJ20100046.
38. Bugge TH, Antalis TM, Wu Q. 2009. Type II transmembrane serine proteases. J. Biol. Chem. 284:23177–23181. http://dx.doi.org/10.1074/jbc.R109.021006.
39. Donaldson SH, Hirsh A, Li DC, Holloway G, Chao J, Boucher RC, Gabriel SE. 2002. Regulation of the epithelial sodium channel by serine proteases in human airways. J. Biol. Chem. 277:8338–8345. http://dx.doi.org/10.1074/jbc.M105044200.
40. Antalis TM, Bugge TH, Wu Q. 2011. Membrane-anchored serine proteases in health and disease. Prog. Mol. Biol. Transl. Sci. 99:1–50. http://dx.doi.org/10.1016/B978-0-12-385504-6.00001-4.
41. Hatesuer B, Bertram S, Mehnert N, Bahgat MM, Nelson PS, Pöhlman S, Schughart K. 2013. Tmprss2 is essential for influenza H1N1 virus pathogenesis in mice. PLoS Pathog. 9:e1003774. http://dx.doi.org/10.1371/journal.ppat.1003774.
42. Shulla A, Heald-Sargent T, Subramanya G, Zhao J, Perlman S, Gallagher T. 2011. A transmembrane serine protease is linked to the severe acute respiratory syndrome coronavirus receptor and activates virus entry. J. Virol. 85:873–882. http://dx.doi.org/10.1128/JVI.02062-10.
43. Glowacka I, Bertram S, Muller MA, Allen P, Soilleux E, Pfefferle S, Steffen I, Tsegaye TS, He Y, Gnirss K, Niemeyer D, Schneider H, Drosten C, Pohlmann S. 2011. Evidence that TMPRSS2 activates the severe acute respiratory syndrome coronavirus spike protein for membrane fusion and reduces viral control by the humoral immune response. J. Virol. 85:4122–4134. http://dx.doi.org/10.1128/JVI.02232-10.
44. Bertram S, Glowacka I, Muller MA, Lavender H, Gnirss K, Nehlmeier I, Niemeyer D, He Y, Simmons G, Drosten C, Soilleux EJ, Jahn O, Steffen I, Pohlmann S. 2011. Cleavage and activation of the severe acute respiratory syndrome coronavirus spike protein by human airway trypsin-like protease. J. Virol. 85:13363–13372. http://dx.doi.org/10.1128/JVI.05300-11.